Atmos. Chem. Phys. Discuss., 12, 9945–9983, 2012
www.atmos-chem-phys-discuss.net/12/9945/2012/
doi:10.5194/acpd-12-9945-2012

Atmospheric Chemistry and Physics Discussions

Modeling the formation and properties of traditional and non-traditional secondary organic aerosol: problem formulation and application to aircraft exhaust

S. H. Jathar[1,2], **M. A. Miracolo**[2], **A. A. Presto**[2], **P. J. Adams**[1,2,3], **and A. L. Robinson**[1,2,4]

[1]Engineering and Public Policy, Carnegie Mellon University, Pittsburgh PA, USA
[2]Center for Atmospheric Particle Studies, Carnegie Mellon University, Pittsburgh PA, USA
[3]Civil and Environmental Engineering, Carnegie Mellon University, Pittsburgh PA, USA
[4]Mechanical Engineering, Carnegie Mellon University, Pittsburgh PA, USA

Received: 21 March 2012 – Accepted: 12 April 2012 – Published: 18 April 2012

Correspondence to: A. L. Robinson (alr@andrew.cmu.edu)

Published by Copernicus Publications on behalf of the European Geosciences Union.

Abstract

We present a methodology to model secondary organic aerosol (SOA) formation from the photo-oxidation of low-volatility organics (semi-volatile and intermediate volatility organic compounds). The model is parameterized and tested using SOA data collected during two field campaigns that characterized the atmospheric evolution of dilute gas-turbine engine emissions using a smog chamber. Photo-oxidation formed a significant amount of SOA, much of which cannot be explained based on the emissions of traditional, speciated precursors; we refer to this as non-traditional SOA (NT-SOA). The NT-SOA can be explained by emissions of low-volatility organic vapors measured using sorbents. Since these vapors could not be speciated, we employ a volatility-based approach to model NT-SOA formation. We show that the method proposed by Robinson et al. (2007) is unable to explain the timing of NT-SOA formation because it assumes a very modest reduction in volatility of the precursors with every oxidation reaction. In contrast, a Hybrid method, similar to models of traditional SOA formation, assumes a larger reduction in volatility with each oxidation step and results in a better reproduction of NT-SOA formation. The NT-SOA yields estimated for the low-volatility organic vapor emissions are similar to literature data for large *n*-alkanes and other low-volatility organics. The yields vary with fuel composition (JP8 versus Fischer-Tropsch) and engine load (idle versus non-idle). These differences are consistent with the expected contribution of high (aromatics and *n*-alkanes) and low (branched alkanes and oxygenated species) SOA forming species to the exhaust.

1 Introduction

Atmospheric aerosols exert a large influence on climate and public health (Bernstein et al., 2004; IPCC, 2007). Secondary organic aerosol (SOA), defined as the organic particulate mass arising from the oxidation products of gas-phase organic species, accounts for a significant fraction of the submicron atmospheric aerosol mass (Zhang

ACPD
12, 9945–9983, 2012

et al., 2007). Until recently, SOA formation was believed to be dominated by the first-generation oxidation products of high-flux volatile organic compounds (VOCs) such as terpenes and single-ring aromatics. SOA formed from speciated VOCs is defined as traditional SOA (T-SOA) and is explicitly accounted for in chemical transport models. However, these models systematically under-predict organic aerosol levels (Heald et al., 2005; Vutukuru et al., 2006; Johnson et al., 2006; Morris et al., 2006; Dzepina et al., 2009, 2010), especially during photochemically active periods.

Recent laboratory and field studies show that combustion emissions when photo-oxidized form substantial SOA mass, greatly in excess of what can be explained by T-SOA models (Robinson et al., 2007; Grieshop et al., 2009; Hodzic et al., 2010; Miracolo et al., 2011, 2012). Robinson et al. (2007) proposed that a significant part of the unexplained SOA stemmed from the oxidation of low-volatility organic vapors; semi-volatile and intermediate volatility organic compounds (SVOCs and IVOCs). In the remainder of this text, we refer to SVOCs and IVOCs together as primary organic carbon (POCs). POCs are co-emitted by combustion sources but are less volatile than VOCs. However, these emissions are not included in models because the vast majority of them cannot be speciated, they do not contribute significantly to ozone formation, and their measurement requires difficult-to-use sorbents. Fundamentally, POC vapors form SOA in the same manner as VOCs; oxidation adds functional groups to the organic molecule, which reduces the volatility (vapor pressure) of the product and leads to condensation into the particle phase. However, the lower initial volatility of POCs mean that they can have higher SOA yields than VOCs (Lim and Ziemann, 2009; Presto et al., 2010). SOA formed from POC vapors is defined as non-traditional SOA (NT-SOA).

A key attribute of POC vapors is that the vast majority of the mass cannot be speciated with traditional GC-based techniques (Schauer et al., 1999, 2002). Instead it is classified as an unresolved complex mixture (UCM) that is thought to be a complex mixture of branched and cyclic alkanes. The problem is fundamentally caused by the number of isomers growing exponentially with carbon number; these isomers co-elute from the GC-column (Goldstein and Galbally, 2007). Since the molecular identity of the

ACPD
12, 9945–9983, 2012

vast majority of POC vapors cannot be ascertained, SOA formation from these compounds cannot be investigated or modeled in the same manner as traditional speciated SOA precursors (benzene, alpha-pinene, et al.). Instead, NT-SOA models have been based on the volatility of the emissions and a volatility-based oxidation mechanism (Robinson et al., 2007; Dzepina et al., 2009; Murphy and Pandis, 2009; Jathar et al., 2011).

Robinson et al. (2007) proposed a method (Robinson-2007) for NT-SOA formation in which POC vapors react with the hydroxyl radical (OH) to form products that were one order of magnitude lower in volatility than their precursor. Pye and Seinfeld (2010) proposed a single-step mechanism for SVOCs where the products of oxidation were two orders of magnitude lower in volatility than the precursor and used SOA-yield data for naphthalene as a surrogate for all IVOCs. Both methods have been implemented in plume, regional and global chemical transport models and are known to close large gaps between observed and predicted SOA concentrations (Shrivastava et al., 2008; Tsimpidi et al., 2009; Dzepina et al., 2010; Pye and Seinfeld, 2010; Jathar et al., 2011).

However, there are several shortcomings with existing models for NT-SOA formation. First, the parameterizations are based on very limited experimental data. For example, the Robinson-2007 method was fit to measured SOA formation from diesel exhaust; it has been assumed that the same fits can be used to model all emissions (fossil fuel, bio fuel and biomass burning) (Shrivastava et al., 2008; Jathar et al., 2011). The Pye and Seinfeld (2010) method for SVOCs has not been constrained using any laboratory data. They use naphthalene as a surrogate for IVOCs, but IVOC UCM is thought to be mainly composed of branched alkanes. Second, both methods assume that each oxidation reaction reduces the volatility of the precursor by one to two orders of magnitude, which is much less than that required to make SOA from VOCs (Kroll and Seinfeld, 2008). Third, the IVOC emissions are inferred from other source tests. For the Robinson-2007 method they are inferred from gas-particle partitioning data; for the Pye and Seinfeld (2010) method they are estimated by scaling naphthalene emissions.

ACPD
12, 9945–9983, 2012

In this paper, we present a new method (Hybrid method) to represent NT-SOA formation from POC vapors. First we present the theoretical framework which is based on the volatility basis set approach (Donahue et al., 2006) and the work of Pankow (1994) and Odum et al. (1996). Next, the Hybrid method is applied to SOA data from smog chamber experiments conducted on dilute aircraft exhaust. A limitation of smog chamber experiments is that it only captures the evolution of the first few generations of oxidation or about 5–10 % of the time spent by precursors and their products in the atmosphere. Therefore, we focus on the SOA production from only the first generation of oxidation. Although this work focuses on aircraft exhaust, the techniques described can be applied to develop parameterizations for NT-SOA formation from other combustion sources.

2 SOA model formulation

The modeling of both T-SOA and NT-SOA is based on the approach of Pankow (1994) and Odum et al. (1996), which parameterizes smog chamber SOA data using a set of semi-volatile surrogate products. The amount of SOA is defined by the gas-particle partitioning of these surrogate products. While Odum et al. (1996) represented SOA with two surrogate products, more recently, researchers (Hildebrandt et al., 2009; Shakya and Griffin, 2010) have used four or more surrogates expressed using the volatility basis set (VBS) (Donahue et al., 2006). The VBS (Donahue et al., 2006) separates low-volatility organics into logarithmically spaced bins of effective saturation concentration (C^*) between 0.01 to 10^7 $\mu g\,m^{-3}$ at 298 K. C^* (inverse of the Pankow-type partitioning coefficient, K_p) is proportional to the saturation vapor pressure; it is a semi-empirical property that describes the gas-particle partitioning of an organic mixture (Pankow, 1994). The gas-particle partitioning is calculated using absorptive partitioning theory:

ACPD
12, 9945–9983, 2012

$$\zeta_i = \left(1 + \frac{C_i^*}{C_{\mathrm{OA}}}\right)^{-1}$$

$$C_{\mathrm{OA}} = \sum_{i=1}^{N} \zeta_i \times M_i|_{\mathrm{g+p}} \quad (1)$$

where, ζ_i is the fraction of mass in volatility bin "i" in the particulate phase, C_i^* is the effective saturation concentration of bin "i" in $\mu g\,m^{-3}$, C_{OA} is the total particulate OA concentration in $\mu g\,m^{-3}$, $M_i|_{\mathrm{g+p}}$ is the total organic concentration (gas+particle) in bin "i" in $\mu g\,m^{-3}$ and N is the number of basis set bins. The VBS is used to track the concentration of all low-volatility organics (SOA and POC). Although both the SOA formation and POC can be tracked using a single basis set, for this work we use three separate basis sets to separately track different types of material. One VBS tracks the traditional SOA produced from the oxidation of speciated VOC precursors. A second tracks the fresh, unoxidized POC and a third tracks the SOA produced from the oxidation of POC.

T-SOA has traditionally been modeled using a distribution of first-generation, non-reactive surrogate products that were much lower in volatility than their precursor. More recently, multi-generational oxidation of the first-generation products was considered (Lane et al., 2008). Previous work has modeled NT-SOA formation from POC emissions with a simple, volatility-based multi-generational oxidation scheme (Robinson-2007) (Robinson et al., 2007; Shrivastava et al., 2008; Jathar et al., 2011). However, there are two potential shortcomings with this approach for NT-SOA. First, the Robinson-2007 parameterization assumes that each oxidation reaction only reduces the volatility of the precursor by one order of magnitude. However, oxidation reactions form a variety of products with different volatilities; for example the addition of a carbonyl, alcohol, nitrate or acid group creates a product with a volatility approximately 1, 3, 3 or 4 orders of magnitude lower than the precursor (Kroll and Seinfeld, 2008). Therefore, a more

ACPD
12, 9945–9983, 2012

realistic NT-SOA parameterization would distribute the products over a set of volatility bins, with some of the bins having much lower volatility than the precursor species (similar to T-SOA models). Second, the Robinson-2007 parameterization assumes the same reduction in volatility for each generation of oxidation. Recent experiments indicate that the reduction in volatility due to oxidation reactions changes as the molecules become more oxygenated and fragmentation (carbon-carbon scission) becomes important (Chacon-Madrid et al., 2010; Chacon-Madrid and Donahue, 2011; Kroll et al., 2011).

To address these shortcomings, we propose that the first generation of NT-SOA production from the oxidation of POCs be treated similar to T-SOA (with precursor specific parameters) and that multi-generational oxidation be treated the same for all SOA. We call this the Hybrid approach, which enables a single, unified framework to be used to model both T-SOA and NT-SOA. We first describe that framework and then its application to T-SOA and NT-SOA to develop parameterizations for NT-SOA formation.

The framework can be represented using the following equations:

$$\frac{\mathrm{d}[X_j]}{\mathrm{d}t} = -k_{\mathrm{Ox},X_j}[\mathrm{Ox}][X_j] \tag{2}$$

$$\frac{\mathrm{d}[M_i|_{\mathrm{g+p}}]}{\mathrm{d}t} = \underbrace{\sum_j \alpha_{i,j} k_{\mathrm{Ox},X_j}[\mathrm{Ox}][X_j]}_{\text{first-generation products}} + \underbrace{\underbrace{\sum_k^N \beta_{i,k} k_{\mathrm{Ox},M_k}[\mathrm{Ox}][M_k|_{\mathrm{g}}]}_{\text{production}} - \underbrace{k_{\mathrm{Ox},M_i}[\mathrm{Ox}][M_i|_{\mathrm{g}}]}_{\text{loss}}}_{\text{multi-generational oxidation}} \tag{3}$$

Equation (2) represents the first-generation oxidation of SOA precursors (speciated VOC or POC) where k_{Ox,X_j} is the reaction rate between the oxidant [Ox] and SOA precursor $[X_j]$. The index j indicates different precursors, either speciated VOC precursors or volatility bins of the POC distribution. Equation (3) tracks the secondary organic material in each VBS bin "i". $M_i|_{\mathrm{g+p}}$ is the total gas + particle organic mass in the i-th bin of the VBS; its gas-particle partitioning is calculated using Eq. (1). The first term in

ACPD
12, 9945–9983, 2012

Eq. (3) represents the first-generation products formed in bin "i" as result of the precursor oxidation where $\alpha_{i,j}$ is the mass yield for the first-generation oxidation reaction. The second and third terms in Eq. (3) account for the evolution of material in the VBS due to multi-generational oxidation where we assume that only vapors in the VBS ($M|_g$) react. $\beta_{k,i}$ is the mass yield from multi-generational oxidation reactions in bin "k" and $k_{Ox,M}$ is the oxidation rate of vapors in the VBS.

To interpret smog chamber data, the framework (Eqs. 1–3) is implemented in a box model that is comprised of two modules: a T-SOA and a NT-SOA module, both of which are described below. The T-SOA module is based on a standard SOA model (Pankow, 1994; Odum et al., 1996); it uses the speciated VOC emissions and oxidant data to predict the amount of T-SOA that is formed. In the NT-SOA module, the amount of NT-SOA formed is first estimated by subtracting off the predicted T-SOA from the measured SOA. Then, the parameters in Eqs. (1)–(3) are determined by fitting the NT-SOA data.

Defining the NT-SOA by difference effectively assumes that the T-SOA module is correct. However, published yields for T-SOA precursors (e.g., toluene) vary by more than a factor of two (Ng et al., 2007; Lane et al., 2008; Hildebrandt et al., 2009). As discussed below, the T-SOA model used for this work is based on an upper end of the published data and therefore the difference approach may systematically underestimate NT-SOA.

2.1 Traditional SOA (T-SOA)

We define T-SOA as the SOA mass formed through the oxidation of speciated VOC precursors. To simulate T-SOA, X_j in Eq. (2) represents an individual precursor (e.g., benzene, toluene, *n*-dodecane, or cyclohexane) and OH is assumed to be the only oxidant. We use the SAPRC 2007 lumping and the mass-yields ($\alpha_{i,j}$ in Eq. 2) proposed by Murphy and Pandis (2010) for all the speciated VOC precursors listed in Table 2. The mass yields are at the high end of those reported in literature; therefore the T-SOA prediction is an upper bound estimate, which, in turn, results in a lower bound estimate for NT-SOA. The lumping and parameters ($k_{Ox,Xj}$ and $\alpha_{i,j}$) for the T-SOA model are

ACPD
12, 9945–9983, 2012

provided in Tables S1 and S2 (Supplement). Figure 1a shows a schematic for the T-SOA model.

To treat multi-generational oxidation of T-SOA, we use the parameterizations recently applied to anthropogenic SOA in regional and global models (Shrivastava et al., 2008, 2009; Murphy and Pandis, 2010; Farina et al., 2010). Gas-phase mass of the T-SOA products reacts with the OH radical ($k_{Ox,M} = 1 \times 10^{-11}\,cm^3\,molecules^{-1}\,s^{-1}$) to form a product that is one order of magnitude lower in volatility than the precursor or shifted by one C^* bin relative to the precursor. To account for the addition of oxygen, 7.5 % of the precursor's mass is added to the product. Hence, for T-SOA, the $\beta_{i,k}$ in Eq. (3) takes the form:

$$\beta_{i,k} = \begin{cases} +1.075 & \text{if} \quad k = i+1\,; \\ 0 & \text{otherwise} \end{cases} \tag{4}$$

2.2 Non-traditional SOA (NT-SOA)

NT-SOA is defined as the SOA mass formed through the oxidation of unspeciated POCs. The mass of NT-SOA is the difference between the measured SOA and the predicted T-SOA. In this section, we present two different approaches to parameterize the NT-SOA formation using the VBS framework (Eqs. 1–3). The methods differ in whether and how they account for first-generation oxidation and ongoing multi-generational oxidation (see Fig. 1b, c).

2.2.1 Robinson-2007 method

Robinson et al. (2007) proposed a simple method to model NT-SOA formation, which uses a single oxidation kernel for all POC oxidation reactions. This method omits a detailed description of the volatility distribution of first-generation products and instead includes only a simple, multi-generational oxidation scheme. The scheme is shown schematically in Fig. 1b.

ACPD
12, 9945–9983, 2012

The simplest way to implement this scheme is to place the volatility-resolved POC precursor mass (X_j) directly into the corresponding VBS (M_i) and eliminating Eq. (2) and the first term in Eq. (3). Similar to the treatment of multi-generational oxidation for T-SOA (Lane et al., 2008), any gas-phase mass in the VBS is reacted with the OH radical to form a product that is in a lower volatility bin than its precursor. For NT-SOA (Robinson-2007), $\beta_{i,k}$ takes the form:

$$\beta_{i,k} = \begin{cases} +(1 + f_{oxy}) & \text{if} \quad k = i + q\,; \\ 0 & \text{otherwise} \end{cases} \tag{5}$$

where, q is the shift in volatility for the product and f_{oxy} is the fraction of oxygen added to the product per reaction.

To simulate SOA formation using the Robinson-2007 method, one must define $k_{Ox,M}$, f_{oxy} and q. Robinson et al. (2007) and Shrivastava et al. (2008) used a $k_{Ox,M}$ of 4×10^{-11} cm^3 molecules^{-1} s^{-1}, a f_{oxy} of 0.075 and a q of 1 based on SOA data for diesel exhaust. Grieshop et al. (2009a) proposed a $k_{OH,M}$ of 4×10^{-11} cm^3 molecules^{-1} s^{-1}, a f_{oxy} of 0.40 a q of 2 based on SOA data for dilute woodsmoke. Dzepina et al. (2009, 2010) and Hodzic et al. (2010) have applied these parameterizations to simulate SOA formation over Mexico City. In addition to evaluating the previously proposed sets of $k_{OH,M}$, f_{oxy} and q values, we also fit the NT-SOA data to determine an optimum set of values for these parameters.

2.2.2 Hybrid method

The Hybrid method is similar to the previously discussed T-SOA model. The first-generation of NT-SOA formation is parameterized by fitting Eqs. (1)–(3) to smog chamber data. A generic scheme is used for multigenerational oxidation. The allows for a more physically realistic treatment of the first-generation oxidation that better represents known effects of photochemical aging on volatility. The Hybrid scheme is shown schematically in Fig. 1c.

ACPD
12, 9945–9983, 2012

In the Hybrid scheme, for the first generation of oxidation, the volatility-resolved POC emissions are treated as precursors or as X_j in Eq. (2) and are assumed to react only with the OH radical. We assume that k_{Ox,X_j} is 4×10^{-11} cm^3 molecules^{-1} s^{-1} for POCs with a $C^* < 10^4$ µg m^{-3} and 3×10^{-11} cm^3 molecules^{-1} s^{-1} for POCs with a $C^* \geq 10^4$ µg m^{-3} based on reactivity data for organics in these volatility ranges (C_{12+} isoalkanes, C_{10+} cycloalkanes, multi-ring aromatics) (Atkinson and Arey, 2003).

The mass-yield matrix ($\alpha_{i,j}$ in Eq. 3) for the Hybrid method is derived by fitting the NT-SOA data. Since there are ten precursors ($C^* = 0.01$ to 10^7 µg m^{-3}; Table 2) and each precursor's products are fit across 4 VBS bins, the Hybrid method potentially requires 40 free parameters (many more than can be constrained with the data). Presto et al. (2010), following the work of Lim and Ziemann (2009), found that for *n*-alkanes, the addition of 2 carbon atoms to an *n*-alkane shifted its corresponding SOA product distribution, on average, by one C^* bin or one order of magnitude in C^* space. Therefore, we assume the same product distribution arising from each POC precursor, but shifted in volatility space by one order of magnitude. This approach reduces the number of free parameters to four. For instance, if [a_1 b_1 c_1 d_1] represents the mass yield for the precursor $C^* = 10^6$ µg m^{-3} across C^* bins [1 10 100 1000] (µg m^{-3}), the mass-yield

ACPD
12, 9945–9983, 2012

matrix $\alpha_{i,j}$ would take the form,

$$\alpha_{i,j} =$$

Products \ Precursors	C*=10^{-2}	C*=10^{-1}	C*=10^{0}	C*=10^{1}	C*=10^{2}	C*=10^{3}	C*=10^{4}	C*=10^{5}	C*=10^{6}	C*=10^{7}
C*=10^{-8}	a_1	-	-	-	-	-	-	-	-	-
C*=10^{-7}	b_1	a_1	-	-	-	-	-	-	-	-
C*=10^{-6}	c_1	b_1	a_1	-	-	-	-	-	-	-
C*=10^{-5}	d_1	c_1	b_1	a_1	-	-	-	-	-	-
C*=10^{-4}	-	d_1	c_1	b_1	a_1	-	-	-	-	-
C*=10^{-3}	-	-	d_1	c_1	b_1	a_1	-	-	-	-
C*=10^{-2}	-	-	-	d_1	c_1	b_1	a_1	-	-	-
C*=10^{-1}	-	-	-	-	d_1	c_1	b_1	a_1	-	-
C*=10^{0}	-	-	-	-	-	d_1	c_1	b_1	a_1	-
C*=10^{1}	-	-	-	-	-	-	d_1	c_1	b_1	a_1
C*=10^{2}	-	-	-	-	-	-	-	d_1	c_1	b_1
C*=10^{3}	-	-	-	-	-	-	-	-	d_1	c_1
C*=10^{4}	-	-	-	-	-	-	-	-	-	d_1

(6)

For multi-generational oxidation, we use the same set of parameters used to model the multi-generational oxidation of T-SOA (Eq. 4).

3 Experimental data

3.1 Overview of experimental methods

The SOA modeling is performed on data from smog chamber experiments conducted on diluted emissions from two different gas-turbine aircraft engines. Here, we provide a brief overview of both field campaigns; further details can be found in Miracolo

ACPD
12, 9945–9983, 2012

et al. (2011), Presto et al. (2011), Miracolo et al. (2012) and Drozd et al. (2012). The first study investigated SOA formation from dilute emissions from a CFM56-2B gas turbine engine operating on Jet Propellant – 8 (JP8) fuel (Presto et al., 2011; Miracolo et al., 2011) at four different engine loads (4 % – ground idle, 7 % – idle/taxing, 30 % – landing and 85 % – takeoff). In the second study, experiments were conducted on dilute emissions from a T63 gas turboshaft engine operating on JP8, Fischer-Tropsch (FT) and JP8/FT 50 : 50 blend fuels at idle and cruise loads. The experiments used in this work are listed in Table 1, along with the naming convention used in the paper.

Briefly, the experiments involved collecting emissions from about 1-m downstream of the engine exit plane and then transferring them through a heated transfer line into a portable Teflon smog chamber. The emissions were diluted with clean (HEPA- and activated-carbon filter) air to achieve concentration levels in the chamber that were representative of downstream of the engine exit plane. To initiate photo-oxidation, the chamber was exposed to natural or artificial sunlight; a suite of instruments tracked the evolution of the gas- and particle-phase pollutants.

3.2 Overview of PM and SOA data

Figure 2 compiles the primary (black carbon and primary organic aerosol or POA) and secondary PM (sulfate and SOA) data from the two field campaigns. The secondary PM data were measured after three to four hours of oxidation inside the smog chamber at typical atmospheric OH concentrations. The sum of the measured primary PM emissions and secondary PM formation spans two orders of magnitude (60–4300 mg kg – fuel^{-1}) and is a strong function of the engine type, load and fuel. These variations are discussed in detail in companion publications (Presto et al., 2011; Miracolo et al., 2011, 2012; Presto et al., 2012; Drozd et al., 2012); here the focus is on modeling the SOA formation measured in the smog chamber. Briefly, at the end of every experiment, the wall-loss corrected secondary PM formation exceeds the direct primary PM emissions, by as much as a factor of 75. Further SOA accounts for more than half of the secondary PM mass (remainder is sulfate) except for in the CFM56-

ACPD
12, 9945–9983, 2012

JP8-Takeoff and T63-FT-Cruise experiments and more than three quarters of the PM mass in the idle experiments. On average, the T63 engine has higher emissions and higher secondary PM formation than the CFM56 engine. Both the SOA formation and precursor emissions decrease substantially with increasing engine load, i.e. idle vs takeoff and idle vs cruise.

3.3 Measured SOA precursors

Simulating SOA formation requires detailed information on SOA precursor concentrations. Table 2 reports VOC and POC (IVOC and SVOC) emissions data for the different experiments. The VOC data were measured using SUMMA canisters and analyzed using a GC-MS. VOC measurements were only made for one of three CFM56-JP8-Idle experiments and the measured VOC emission profile was applied to the other two experiments. For the CFM56-JP8-Taxi and CFM56-JP8-Landing experiments, only a small number of VOCs were measured (Presto et al., 2011) and therefore we estimated emissions of additional VOCs using data from the APEX study (Wey et al., 2006). The VOC emissions at taxi were assumed to be 40 % of those at idle and VOC emissions at landing were assumed to be the same as those at takeoff.

POC emissions were characterized by GC-MS analysis of quartz filter and Tenax TA sorbent tube samples (Presto et al., 2011). Formally, we define POC as the sum of unspeciated emissions that have a C^* lower than or equal to $10^7\,\mu g\,m^{-3}$. Presto et al. (2011) speciated less than 10 % of the POC emissions (similar to studies done with other sources Schauer et al., 1999, 2002) the remainder was reported as an unresolved complex mixture (UCM). To estimate the total mass of POC emissions, Presto et al. (2011) developed a calibration curve for the UCM mass using fuel and lubricating oil used by the aircraft. The emissions were then distributed into the VBS based on the GC elution time (Presto et al., 2012). Table 2 reports measured POC emissions as a function of C^*.

Figure 3 plots the measured SOA and its precursors – POC and speciated VOC – for the different experiments. The VOCs include only those that form SOA based on

ACPD
12, 9945–9983, 2012

the SAPRC07 classification. Apart from the T63-JP8-Cruise experiment, the measured SOA is smaller than the sum of the precursors (POC + VOC). It is likely that the precursors in the T63-JP8-Cruise experiment are mostly oxygenated species and therefore not accounted for in Fig. 3 because our instrumentation largely targets hydrocarbons and modestly polar species. The POC emissions, on average, are larger than the speciated SOA precursors and therefore likely to be very important SOA precursors. Most of the POC emissions are IVOCs.

3.4 Oxidant concentrations

The vast majority of the SOA precursors in aircraft exhaust are saturated species (there are significant unsaturated light VOCs); therefore the oxidation chemistry in the smog chamber experiments are largely driven by the hydroxyl radical (OH) and not by ozone. OH concentrations were not directly measured but inferred from the measured decay of organic (e.g., toluene) and inorganic (e.g., SO_2) species. For some experiments, we estimated the OH exposure only using high reactivity species ($k_{OH} > 10^{-11}\,cm^3\,molecules^{-1}\,s^{-1}$) to reduce uncertainties associated with any bag leakage. Figure S1 shows the median OH exposure (orange cross) with the standard error of the mean (green bars) calculated for each experiment. The OH exposure ranges from 4 to almost 50 h of atmospheric oxidation at a typical OH concentration of $10^6\,molecules\,cm^{-3}$.

4 Results

4.1 T-SOA

Model predictions for T-SOA are compared to the measured SOA in Fig. 4a. Each point represents a time-averaged value over 100 s from an individual experiment. The CFM56 and T63 data are presented in separate panels. The model predicts that

ACPD
12, 9945–9983, 2012

aromatics are the most important T-SOA precursors. In order to quantify the model-measurement comparison, we calculate the fractional error:

$$\text{Fractional Error} = \frac{1}{N}\sum_{i=1}^{N}\frac{|P-M|}{\frac{P+M}{2}} \quad (7)$$

where P is the predicted OA, M is the measured OA mass and N is number of data points. Fractional error values are listed in Fig. 4a. Except for the CFM56-JP8-Takeoff and T63-FT-Idle experiments, the T-SOA module predicts about half of the measured SOA. We hypothesize that the large unexplained SOA is a direct result of unspeciated POC oxidation and is hereon referred to as NT-SOA.

4.2 NT-SOA formed versus POC reacted

The NT-SOA is estimated by subtracting the T-SOA prediction from the measured SOA. Except for the T63-FT experiments, NT-SOA accounts for anywhere between 30 and 96 % of the SOA measured in the chamber. Although the T-SOA model explains essentially all of the SOA formed in the T63-FT experiments, the mass yields of Murphy and Pandis (2010) are at the high end of those reported in the literature and therefore the T-SOA model may overestimate T-SOA.

Before applying the NT-SOA models, we first evaluate a mass balance between the estimated NT-SOA and the estimated mass of reacted POC. For this calculation, we assume that the POCs with $C^* < 10^4\,\mu g\,m^{-3}$ react with the OH radical with a reactivity of $4\times10^{-11}\,cm^3\,molecules^{-1}\,s^{-1}$ and POCs with $C^* \geq 10^4\,\mu g\,m^{-3}$ react with the OH radical with a reactivity of $3\times10^{-11}\,cm^3\,molecules^{-1}\,s^{-1}$. To quantify the mass balance, we calculate an effective NT-SOA yield, which is defined as follows:

$$\text{Effective NT-SOA Yield} = \frac{\text{NT-SOA formed}}{\text{POC reacted}} \quad (8)$$

Figure 5 plots the effective NT-SOA yield as a function of the OA concentration (C_{OA}). There are several important points to make from the plot. First, from a mass balance

ACPD
12, 9945–9983, 2012

perspective, the NT-SOA yields are reasonable (i.e., they are less than 1), which means that the amount of NT-SOA formed is less than the amount of POC reacted. Second, the effective NT-SOA yields are similar to published yield data for IVOCs, such as *n*-dodecane and *n*-tridecane (Presto et al., 2010) and large (C_{10+}) branched and cyclic alkanes (Lim and Ziemann, 2009). For the JP8 experiments, the effective NT-SOA yields fall between the measured yields for *n*-dodecane (C_{12}) and *n*-tridecane (C_{13}). This is not surprising since the UCM distribution of both the emissions and unburned fuel peak between C_{11} and C_{15} (Corporan et al., 2011; Presto et al., 2011). Finally, the NT-SOA yields increase with increasing C_{OA}, implying that the NT-SOA is semi-volatile, similar to T-SOA formed in smog chamber experiments (Odum et al., 1996).

The effective yields in Fig. 5 appear to depend on both engine load and fuel composition. The idle experiments appear to have higher yields than non-idle experiments. This could be due to differences in precursor composition; the idle POC emissions are comprised of compounds that more efficiently produce SOA than non-idle emissions. If true, then different NT-SOA parameterizations would need to be developed for different engine loads. Alternatively, the higher idle-experiment yields may also be due to partitioning differences (idle experiments were conducted at higher C_{OA}). The NT-SOA yields for JP8-Idle are higher than Blend-Idle which are higher than FT-Idle. Accounting for differences in C_{OA} values, it could be argued that Blend-Idle yields are an arithmetic average of the JP8-Idle and FT-Idle yields. Miracolo et al. (2012) showed that the differences in SOA formation between JP8 and FT could mostly be attributed to compositional differences in the fuels. FT is mainly comprised of branched alkanes which have low SOA yields versus JP8 which contains much higher yield *n*-alkanes and aromatics. Therefore, different NT-SOA parameterizations may be needed for different fuel types.

ACPD
12, 9945–9983, 2012

4.3 Parameterizing NT-SOA formation

In this section we develop parameterizations for NT-SOA formation by fitting the measured SOA production. The goal is to determine an optimum parameter-set for the Robinson-2007 ($k_{OH,M}$, f_{oxy} and q) and Hybrid approaches ($\alpha_{i,j}$; Eq. 5).

4.3.1 Robinson-2007 method

The Robinson-2007 method, when using the Robinson et al. (2007) and Grieshop et al. (2009) parameter sets, under-predicts the NT-SOA formed during idle-experiments but over-predicts it during non-idle experiments. Therefore, we fit the NT-SOA data to find an optimum parameter set for the Robinson-2007 method. We considered a wide but realistic range of reaction rates (k_{OH}), fraction of oxygen added to the product per reaction (f_{oxy}) and shift in volatility (q). For k_{OH}, we use a range of 1 to 5×10^{-11} cm^3 molecules^{-1} s^{-1} based on Atkinson and Arey (2003). For f_{oxy}, we use a range of 0.05 to 0.4, which corresponds to the addition of 1 to 5 oxygen atoms per generation to a C_{15} alkane. For q, we use a range of 1 to 2, which corresponds to 1 to 2 orders of magnitude change in the product volatility with each oxidation reaction. Within these ranges, the optimum set was determined by minimizing the fractional error (Eq. 5) between model predictions and measurements for each experiment.

For the idle experiments (except for the FT-Idle) an aggressive parameter-set ($k_{OH} = 3–5 \times 10^{-11}$ cm^3 molecules^{-1} s^{-1}, $f_{oxy} = 0.05–0.4$, $q = 2$) is required to reproduce the SOA data. In comparison, a more modest parameter-set ($k_{OH} = 1–3 \times 10^{-11}$ cm^3 molecules^{-1} s^{-1}, $f_{oxy} = 0.05–0.3$, $q = 1$) is sufficient to describe the non-idle SOA data since a lot of the SOA formed in those experiments is explained by T-SOA. The results are illustrated in Fig. 4b, which plots model predictions using the Robinson-2007 method with the best fit for each experiment against the OA measured in the chamber. Compared to predictions from the T-SOA model alone, we see model predictions improve for the CFM56 experiments but only slightly for the T63 experiments. The improvement is quantified by the fractional error values listed in Fig. 4.

ACPD
12, 9945–9983, 2012

Although an optimum parameter set provides some improvement over the T-SOA model, the Robinson-2007 method cannot reproduce the temporal trend in the data. The measured SOA mass varies linearly or rolls over with OH exposure in the chamber (Fig. 6). However, the NT-SOA calculated using the Robinson-2007 method shows the opposite trend with little NT-SOA formed initially and significantly more is formed later. This effect is clearly seen for the T63-Blend-Idle case in Fig. 7. This happens because the Robinson-2007 approach requires several generations of oxidation (a lot of OH exposure) before a large fraction of the products have a C^* low enough to partition into the particle phase. The problem is most severe in the idle experiments where almost all of the emissions are IVOCs (Table 2). The Robinson-2007 method works for the CFM56-JP8-Taxi and CFM56-JP8-Takeoff experiments primarily because a sizeable fraction of the emissions are already found in lower C^* bins ($C^* = 10^2 - 10^4\,\mu g\,m^{-3}$; Table 2).

The O:C ratio of OA reveals additional problems with the Robinson-2007 method. The O:C of the POA is measured before the oxidation phase of the experiment. For T-SOA, we use the work of Chhabra et al. (2010) to assign the O:C for SOA formed from alkenes and aromatics and the work of Presto et al. (2010) to assign the O:C for SOA formed from alkanes. For NT-SOA, we calculate O:C by explicitly tracking the addition of oxygen per reaction (f_{oxy}). For a few of the experiments, the optimum parameter-set for the Robinson-2007 method predicts a very high O:C ratio (> 0.8) of OA. This occurs because precursors have to go through multiple generations of oxidation before they reach a low enough volatility to partition into the particle phase. A consequence of this is that a lot of oxygen is added, with the exact amount depending on the values of f_{oxy} and q. For example, for the optimized parameter-set for the T63-JP8-Idle experiment ($k_{OH} = 5 \times 10^{-11}\,cm^3\,molecules^{-1}\,s^{-1}$, $f_{oxy} = 0.40$, $q = 2$), the O:C of the product would be close to 1 after only two generations of oxidation versus 0.32 for the measured data. It is clear the Robinson-2007 method with a modest reduction in volatility with each oxidation reaction is unable to reproduce both the temporal dependence of NT-SOA and the O:C of OA.

ACPD
12, 9945–9983, 2012

4.3.2 Hybrid method

We fit the NT-SOA data to determine a set of VBS yields (Eq. 5) for the Hybrid parameterization for each experiment individually. Figure 6 plots the time series of measured and predicted OA for each experiment, with the NT-SOA calculated using the best fit for the Hybrid method. The upper and lower bounds of the SOA are presented to indicate experimental uncertainty (we have not accounted for uncertainty in the T-SOA model). The predicted contribution from the first generation of oxidation of POC is labeled "NTSOA (1st generation)" and the contribution from multi-generational oxidation is labeled "NTSOA (aged)". Figure 6 indicates that the multi-generational oxidation – as defined by Eq. (4) – contributes negligibly to the SOA mass over the range of oxidant exposures observed in these experiments. Scatter plots of the model versus measurements are shown in Fig. 4c. The Hybrid method is able to reproduce the data better than the Robinson-2007 method with significantly lower fractional error.

To compare the Hybrid method fits across different experiments, Fig. 8 plots the effective NT-SOA yields for select POC precursors as a function of C_{OA} for the JP8 experiments. The effective yield is defined as the SOA formed by each discrete POC precursor divided by the mass of POC precursor reacted. Figure 8a shows yields for the precursors 10^2 and 10^3 $\mu g\,m^{-3}$ and Fig. 8b shows yields for precursors 10^4, 10^5 and 10^6 $\mu g\,m^{-3}$. For visual clarity, we have excluded points for all POC precursors that contribute less than 15 % to the NT-SOA mass. The lower C^* surrogates generally do not contribute much NT-SOA mass because their emissions are either low and/or because very little of their mass exists as vapors and is therefore available for oxidation.

For all of the idle experiments (Fig. 8b), irrespective of the field campaign, almost all of the NT-SOA is produced from oxidation of IVOCs (C^* bins: 10^5, 10^6 and 10^7 $\mu g\,m^{-3}$). This is expected because 90 % of the POC emissions are IVOCs which peak at $C^* = 10^6$ $\mu g\,m^{-3}$. These emissions appear to be mostly composed of unburned fuel (Miracolo et al., 2012). In contrast, for the non-idle experiments (Fig. 8a), the NT-SOA arises from less volatile POCs in 10^3 and 10^4 $\mu g\,m^{-3}$ bins. We hypothesize that at higher loads the

ACPD
12, 9945–9983, 2012

combustion efficiency is higher and hence the fuel (C^* peak of 10^6 or $10^7\,\mu g\,m^{-3}$) might be partially oxidized to form intermediates that have a slightly lower volatility (10^3 or $10^4\,\mu g\,m^{-3}$).

Figure 8a shows that the effective SOA yields for POCs in the 10^3 and $10^4\,\mu g\,m^{-3}$ bins (symbols) are lower than the published yields for *n*-alkanes (Presto et al., 2010) in the same C^* range (dashed lines; $C_{18} \sim 10^3\,\mu g\,m^{-3}$ and $C_{16} \sim 10^4\,\mu g\,m^{-3}$). This suggests that the unspeciated POC mass in the 10^3 and $10^4\,\mu g\,m^{-3}$ is likely composed of branched and oxygenated compounds which have lower yields than corresponding *n*-alkanes (Lim and Ziemann, 2009). In comparison, Fig. 6b shows that the SOA yields for POCs in the 10^5, 10^6 and $10^7\,\mu g\,m^{-3}$ bins (symbols) are equal or higher than published yields for *n*-alkanes in the same C^* range (dashed lines; $C_{14} \sim 10^5\,\mu g\,m^{-3}$, $C_{12} \sim 10^6\,\mu g\,m^{-3}$ and $C_{10} \sim 10^7\,\mu g\,m^{-3}$). Therefore, the unspeciated POC mass in the 10^5, 10^6 and $10^7\,\mu g\,m^{-3}$ bins is likely composed of cycloalkanes, alkylbenzenes and polycyclic aromatics which have higher yields than *n*-alkanes (Ng et al., 2007; Hildebrandt et al., 2009). This seems consistent with the emissions in these bins being comprised of unburned fuel when the engine is idling.

5 Conclusions and discussion

In this work, we investigated the potential contribution of low-volatility organic vapors to SOA formation in dilute aircraft exhaust. First, we showed that unspeciated low-volatility organic vapors (POC; S/IVOC) are important classes of SOA precursors in aircraft exhaust since they accounted, in most cases, for more than half of the measured SOA. Second, we demonstrated that the method proposed by Robinson et al. (2007) to model NT-SOA formation does not have a large enough volatility shift to reproduce the temporal evolution of the SOA production. Third, we developed a new method (Hybrid) to model NT-SOA (similar to traditional SOA models) that separated the first generation of oxidation – which was constrained using laboratory data – from future generations

ACPD
12, 9945–9983, 2012

of oxidation. To explain the measured data, the first generation of oxidation produces much lower volatility products than the Robinson et al. (2007) approach and therefore provides a realistic representation of chemistry.

In addition to varying with organic aerosol concentration, the NT-SOA yields appear to be a function of both the (a) fuel composition and (b) engine load. This is not surprising since both molecular structure in addition to volatility influences SOA yields (Lim and Ziemann, 2009). For example, the effective NT-SOA yield is highest for JP8 and lowest for FT while the 50:50 blend appears to be an average of JP8 and FT. JP8 consists mostly of straight/cyclic alkanes (53 %) and aromatics (17 %), which form more SOA than branched alkanes that mostly constitute FT (88 %) (Lim and Ziemann, 2009). The effective NT-SOA yields also appear to be higher for JP8 idle emissions than for JP8 non-idle emissions. Therefore, the NT-SOA yields also appear to depend on engine load, again, presumably due to differences in precursor composition. The idle emissions appear to be comprised of unburned alkanes and aromatic compounds found in the fuel which have higher SOA yields than the non-idle emissions, which appear to be comprised of partially burned fuel. Therefore, different NT-SOA parameterizations may be needed for different fuels and different engine loads.

Table 3 provides Hybrid-parameterizations determined in this work for aircraft emissions. They are suitable for use with the VBS framework in any box, plume, regional or global OA model in conjunction with the emissions data listed in Table 2. Although the emissions data are representative of specific engines, emissions data for another gas-turbine engine could be estimated by scaling the emissions (both VOC and POC) using a high-flux species like acetylene, propene or benzene. For different engine loads, we use the JP8 non-idle experiments to determine a mass yield matrix ($\alpha_{i,j}$) for JP8 non-idle emissions and the JP8 idle experiments to determine a mass yield matrix ($\alpha_{i,j}$) for JP8 idle emissions. Figure S2 indicates reasonable model-measurement comparison when the JP8 non-idle mass yield matrix is used for the JP8 non-idle experiments and JP8 idle mass yield matrix is used for the JP8 idle experiments.

ACPD
12, 9945–9983, 2012

Future research is needed to extend the methods developed here to model SOA formation from other combustion sources.

Supplementary material related to this article is available online at: http://www.atmos-chem-phys-discuss.net/12/9945/2012/acpd-12-9945-2012-supplement.pdf.

Acknowledgements. Funding was provided by the US Department of Defense Strategic Environmental Research and Development Program (SERDP) under project WP-1626. The views, opinions, and/or findings contained in this paper are those of the authors and should not be construed as an official position of any of the funding agency.

References

Atkinson, R. and Arey, J.: Atmospheric degradation of volatile organic compounds, Chem. Rev., 103, 4605–4638, 2003.

Bernstein, J. A., Alexis, N., Barnes, C., Bernstein, I. L., Bernstein, J. A., Nel, A., Peden, D., Diaz-Sanchez, D., Tarlo, S. M., and Williams, P. B.: Health effects of air pollution, J. Allergy Clin. Immun., 114, 1116–1123, 2004.

Chacon-Madrid, H. J. and Donahue, N. M.: Fragmentation vs. functionalization: chemical aging and organic aerosol formation, Atmos. Chem. Phys., 11, 10553–10563, doi:10.5194/acp-11-10553-2011, 2011.

Chacon-Madrid, H. J., Presto, A. A., and Donahue, N. M.: Functionalization vs. fragmentation: *n*-aldehyde oxidation mechanisms and secondary organic aerosol formation, Phys. Chem. Chem. Phys., 12, 13975–13982, doi:10.1039/c0cp00200c, 2010.

Corporan, E., Edwards, T., Shafer, L., DeWitt, M. J., Klingshirn, C., Zabarnick, S., West, Z., Striebich, R., Graham, J., and Klein, J.: Chemical, thermal stability, seal swell, and emissions studies of alternative jet fuels, Energ. Fuels, 25, 955–966, doi:10.1021/ef101520v, 2011.

Donahue, N., Robinson, A., Stanier, C., and Pandis, S.: Coupled partitioning, dilution, and chemical aging of semivolatile organics, Environ. Sci. Technol, 40, 2635–2643, doi:10.1021/es052297c, 2006.

ACPD
12, 9945–9983, 2012

Drozd, G. T., Miracolo, M. A., Presto, A. A., Corporan, E., Lipsky, E. M., and Robinson, A. L.: Particulate and organic vapor emissions from an in-use helicopter engine, in preparation, 2012.

Dzepina, K., Volkamer, R. M., Madronich, S., Tulet, P., Ulbrich, I. M., Zhang, Q., Cappa, C. D., Ziemann, P. J., and Jimenez, J. L.: Evaluation of recently-proposed secondary organic aerosol models for a case study in Mexico City, Atmos. Chem. Phys., 9, 5681–5709, doi:10.5194/acp-9-5681-2009, 2009.

Dzepina, K., Cappa, C. D., Volkamer, R. M., Madronich, S., DeCarlo, P. F., Zaveri, R. A., and Jimenez, J. L.: Modeling the multiday evolution and aging of secondary organic aerosol during milagro 2006, Environ. Sci. Technol., 45, 3496–3503, doi:10.1021/es103186f, 2010.

Farina, S. C., Adams, P. J., and Pandis, S. N.: Modeling global secondary organic aerosol formation and processing with the volatility basis set: Implications for anthropogenic secondary organic aerosol, J. Geophys. Res., 115, D09202, doi:10.1029/2009JD013046, 2010.

Goldstein, A. H. and Galbally, I. E.: Known and unexplored organic constituents in the earth's atmosphere, Environ. Sci. Technol., 41, 1514–1521, doi:10.1021/es072476p, 2007.

Grieshop, A. P., Donahue, N. M., and Robinson, A. L.: Laboratory investigation of photochemical oxidation of organic aerosol from wood fires 2: analysis of aerosol mass spectrometer data, Atmos. Chem. Phys., 9, 2227–2240, doi:10.5194/acp-9-2227-2009, 2009.

Heald, C. L., Jacob, D. J., Park, R. J., Russell, L. M., Huebert, B. J., Seinfeld, J. H., Liao, H., and Weber, R. J.: A large organic aerosol source in the free troposphere missing from current models, Geophys. Res. Lett., 32, L18809, doi:10.1029/2005GL023831, 2005.

Hildebrandt, L., Donahue, N. M., and Pandis, S. N.: High formation of secondary organic aerosol from the photo-oxidation of toluene, Atmos. Chem. Phys., 9, 2973–2986, doi:10.5194/acp-9-2973-2009, 2009.

Hodzic, A., Jimenez, J. L., Madronich, S., Canagaratna, M. R., DeCarlo, P. F., Kleinman, L., and Fast, J.: Modeling organic aerosols in a megacity: potential contribution of semi-volatile and intermediate volatility primary organic compounds to secondary organic aerosol formation, Atmos. Chem. Phys., 10, 5491–5514, doi:10.5194/acp-10-5491-2010, 2010.

IPCC: Technical Summary, in: Climate Change 2007: The Physical Science Basis. Contribution of Working Group I to the Fourth Assessment Report of the Intergovernmental Panel on Climate Change, edited by: Solomon, S., Qin, D., Manning, M., Alley, R. B., Berntsen, T., Bindoff, N. L., Chen, Z., Chidthaisong, A., Gregory, J. M., Hegerl, G. C., Heimann, M., Hewitson, B., Hoskins, B. J., Joos, F., Jouzel, J., Kattsov, V., Lohmann, U., Matsuno, T., Molina, M.,

ACPD
12, 9945–9983, 2012

Nicholls, N., Overpeck, J., Raga, G., Ramaswamy, V., Ren, J., Rusticucci, M., Somerville, R., Stocker, T. F., Whetton, P., Wood, R. A., and Wratt, D., Cambridge University Press, Cambridge, United Kingdom and New York, NY, USA, 2007.

Jathar, S. H., Farina, S. C., Robinson, A. L., and Adams, P. J.: The influence of semi-volatile and reactive primary emissions on the abundance and properties of global organic aerosol, Atmos. Chem. Phys., 11, 7727–7746, doi:10.5194/acp-11-7727-2011, 2011.

Johnson, D., Utembe, S. R., Jenkin, M. E., Derwent, R. G., Hayman, G. D., Alfarra, M. R., Coe, H., and McFiggans, G.: Simulating regional scale secondary organic aerosol formation during the TORCH 2003 campaign in the southern UK, Atmos. Chem. Phys., 6, 403–418, doi:10.5194/acp-6-403-2006, 2006.

Kroll, J. H. and Seinfeld, J. H.: Chemistry of secondary organic aerosol: formation and evolution of low-volatility organics in the atmosphere, Atmos. Environ., 42, 3593–3624, 2008.

Kroll, J. H., Donahue, N. M., Jimenez, J. L., Kessler, S. H., Canagaratna, M. R., Wilson, K. R., Altieri, K. E., Mazzoleni, L. R., Wozniak, A. S., Bluhm, H., Mysak, E. R., Smith, J. D., Kolb, C. E., and Worsnop, D. R.: Carbon oxidation state as a metric for describing the chemistry of atmospheric organic aerosol, Nat. Chem., 3, 133–139, 2011.

Lane, T. E., Donahue, N. M., and Pandis, S. N.: Simulating secondary organic aerosol formation using the volatility basis-set approach in a chemical transport model, Atmos. Environ., 42, 7439–7451, 2008.

Lim, Y. B. and Ziemann, P. J.: Chemistry of secondary organic aerosol formation from oh radical-initiated reactions of linear, branched, and cyclic alkanes in the presence of NO_x, Aerosol Sci. Technol., 43, 604–619, 2009.

Miracolo, M. A., Hennigan, C. J., Ranjan, M., Nguyen, N. T., Gordon, T. D., Lipsky, E. M., Presto, A. A., Donahue, N. M., and Robinson, A. L.: Secondary aerosol formation from photochemical aging of aircraft exhaust in a smog chamber, Atmos. Chem. Phys., 11, 4135–4147, doi:10.5194/acp-11-4135-2011, 2011.

Miracolo, M. A., Drozd, G. T., Jathar, S. H., Presto, A. A., Lipsky, E. M., Corporan, E., and Robinson, A. L.: Fuel composition and secondary organic aerosol formation: gas-turbine exhaust and alternative aviation fuels, Environ. Sci. Technol., submitted, 2012.

Morris, R. E., Koo, B., Guenther, A., Yarwood, G., McNally, D., Tesche, T. W., Tonnesen, G., Boylan, J., and Brewer, P.: Model sensitivity evaluation for organic carbon using two multi-pollutant air quality models that simulate regional haze in the Southeastern United States, Atmos. Environ., 40, 4960–4972, 2006.

ACPD
12, 9945–9983, 2012

Murphy, B. and Pandis, S.: Simulating the formation of semivolatile primary and secondary organic aerosol in a regional chemical transport model, Environ. Sci. Technol., 43, 4722–4728, doi:10.1021/es803168a, 2009.

Murphy, B. N. and Pandis, S. N.: Exploring summertime organic aerosol formation in the Eastern United States using a regional-scale budget approach and ambient measurements, J. Geophys. Res., 115, D24216, doi:10.1029/2010JD014418, 2010.

Ng, N. L., Kroll, J. H., Chan, A. W. H., Chhabra, P. S., Flagan, R. C., and Seinfeld, J. H.: Secondary organic aerosol formation from *m*-xylene, toluene, and benzene, Atmos. Chem. Phys., 7, 3909–3922, doi:10.5194/acp-7-3909-2007, 2007.

Odum, J. R., Hoffmann, T., Bowman, F., Collins, D., Flagan, R. C., and Seinfeld, J. H.: Gas/particle partitioning and secondary organic aerosol yields, Environ. Sci. Technol., 30, 2580–2585, 1996.

Pankow, J. F.: An absorption model of gas/particle partitioning of organic compounds in the atmosphere, Atmos. Environ., 28, 185–188, 1994.

Presto, A. A., Miracolo, M. A., Donahue, N. M., and Robinson, A. L.: Secondary organic aerosol formation from high-NO_x photo-oxidation of low volatility precursors: *n*-alkanes, Environ. Sci. Technol., 44, 2029–2034, 2010.

Presto, A. A., Nguyen, N. T., Ranjan, M., Reeder, A. J., Lipsky, E. M., Hennigan, C. J., Miracolo, M. A., Riemer, D. D., and Robinson, A. L.: Fine particle and organic vapor emissions from staged tests of an in-use aircraft engine, Atmos. Environ., 45, 3603–3612, 2011.

Presto, A. A., Hennigan, C. J., Nguyen, N. T., and Robinson, A. L.: Determination of volatility distributions of primary organic aerosol emissions from combustion systems using thermal desorption gas chromatography mass spectrometry, Aerosol Sci. Technol., submitted, 2012.

Pye, H. O. T. and Seinfeld, J. H.: A global perspective on aerosol from low-volatility organic compounds, Atmos. Chem. Phys., 10, 4377–4401, doi:10.5194/acp-10-4377-2010, 2010.

Robinson, A. L., Donahue, N. M., Shrivastava, M. K., Weitkamp, E. A., Sage, A. M., Grieshop, A. P., Lane, T. E., Pierce, J. R., and Pandis, S. N.: Rethinking organic aerosols: semivolatile emissions and photochemical aging, Science, 315, 1259–1262, 2007.

Schauer, J. J., Kleeman, M. J., Cass, G. R., and Simoneit, B. R. T.: Measurement of emissions from air pollution sources. 2. C_1 through C_30 organic compounds from medium duty diesel trucks, Environ. Sci. Technol., 33, 1578–1587, 1999.

ACPD
12, 9945–9983, 2012

Schauer, J. J., Kleeman, M. J., Cass, G. R., and Simoneit, B. R. T.: Measurement of emissions from air pollution sources. 5. C1-c32 organic compounds from gasoline-powered motor vehicles, Environ. Sci. Technol., 36, 1169–1180, 2002.

Shakya, K. M. and Griffin, R. J.: Secondary organic aerosol from photooxidation of polycyclic aromatic hydrocarbons, Environ. Sci. Technol., 44, 8134–8139, doi:10.1021/es1019417, 2010.

Shrivastava, M. K., Lane, T. E., Donahue, N. M., Pandis, S. N., and Robinson, A. L.: Effects of gas particle partitioning and aging of primary emissions on urban and regional organic aerosol concentrations, J. Geophys. Res.-Atmos., 113, D18301, doi:10.1029/2007JD009735, 2008.

Tsimpidi, A. P., Karydis, V. A., Zavala, M., Lei, W., Molina, L., Ulbrich, I. M., Jimenez, J. L., and Pandis, S. N.: Evaluation of the volatility basis-set approach for the simulation of organic aerosol formation in the Mexico City metropolitan area, Atmos. Chem. Phys., 10, 525–546, doi:10.5194/acp-10-525-2010, 2010.

Vutukuru, S., Griffin, R. J., and Dabdub, D.: Simulation and analysis of secondary organic aerosol dynamics in the south coast air basin of california, J. Geophys. Res., 111, D10S12, doi:10.1029/2005JD006139, 2006.

Wey, C., Anderson, B., Hudgins, C., Wey, C., Li-Jones, X., Winstead, E., Thornhill, L., Lobo, P., Hagen, D., and Whitefield, P.: Aircraft particle emissions experiment (APEX), NASA TM-2006, 2006.

Zhang, Q., Jimenez, J. L., Canagaratna, M. R., Allan, J. D., Coe, H., Ulbrich, I., Alfarra, M. R., Takami, A., Middlebrook, A. M., Sun, Y. L., Dzepina, K., Dunlea, E., Docherty, K., DeCarlo, P. F., Salcedo, D., Onasch, T., Jayne, J. T., Miyoshi, T., Shimono, A., Hatakeyama, S., Takegawa, N., Kondo, Y., Schneider, J., Drewnick, F., Borrmann, S., Weimer, S., Demerjian, K., Williams, P., Bower, K., Bahreini, R., Cottrell, L., Griffin, R. J., Rautiainen, J., Sun, J. Y., Zhang, Y. M., and Worsnop, D. R.: Ubiquity and dominance of oxygenated species in organic aerosols in anthropogenically-influenced Northern Hemisphere midlatitudes, Geophys. Res. Lett, 34, L13801, doi:10.1029/2007GL029979, 2007.

ACPD
12, 9945–9983, 2012

Table 1. List of smog chamber experiments conducted at the 171st Air Refueling Wing in Pittsburgh and Wright-Patterson Air Force Base.

Number	Experiment name	Engine	Load	Fuel
1	CFM56-JP8-Idle(1)	CFM56–2B	4 %	JP8
2	CFM56-JP8-Idle(2)	CFM56–2B	4 %	JP8
3	CFM56-JP8-Idle(3)	CFM56–2B	4 %	JP8
4	CFM56-JP8-Taxi	CFM56–2B	7 %	JP8
5	CFM56-JP8-Landing	CFM56–2B	30 %	JP8
6	CFM56-JP8-Takeoff	CFM56–2B	85 %	JP8
7	T63-JP8-Idle	T63	Idle	JP8
8	T63-FT-Idle(1)	T63	Idle	FT
9	T63-FT-Idle(2)	T63	Idle	FT
10	T63-Blend-Idle	T63	Idle	JP8 : FT Blend
11	T63-JP8-Cruise	T63	Cruise	JP8
12	T63-FT-Cruise	T63	Cruise	FT

ACPD
12, 9945–9983, 2012

Table 2. Emission factor (mg kg-fuel^{-1}) for speciated VOCs and POCs for each engine, fuel and engine load.

	Species	CFM56-JP8				T63-JP8		T63-FT		T63-Blend
		Idle	Taxi	Landing	Takeoff	Idle	Cruise	Idle	Cruise	Idle
VOC	1-butene	194.6	58.4	2.2	2.2	388.6	1.2	155.2	1.4	379.3
	1-heptene	61.5	18.5	–	–	0.1	0.0	6.2	0.0	15.0
	1-hexene	81.1	24.3	–	–	–	–	–	–	–
	1-methylcyclohexene	5.2	1.6	–	–	–	–	–	–	–
	1-octene	5.9	1.8	1.2	1.2	–	–	–	–	–
	1-pentene	91.2	27.4	10.8	10.8	79.2	0.0	67.8	0.0	0.0
	1,2-butadiene	6.4	1.9	–	–	1.4	0.0	4.8	0.0	4.7
	1,2-diethylbenzene	10.9	3.3	1.9	1.9	–	–	–	–	–
	1,2,3-trimethylbenzene	47.0	14.1	1.7	1.7	4.1	0.0	10.5	0.0	42.4
	1,2,4-trimethylbenzene	41.9	12.6	7.4	7.4	24.1	0.0	29.7	0.0	155.3
	1,2,4,5-tetramethylbenzene	27.2	8.2	–	–	–	–	–	–	–
	1,3-butadiene	230.3	69.1	–	–	379.0	2.7	75.2	1.3	0.0
	1,3-diethylbenzene	10.2	3.1	1.8	1.8	14.2	1.1	176.4	0.0	162.5
	1,3,5-trimethylbenzene	14.4	4.3	1.0	1.0	15.9	0.0	38.0	0.0	61.8
	1,4-diethylbenzene	46.7	14.0	1.9	1.9	3.6	3.8	73.7	0.0	88.4
	2-ethyltoluene	12.6	3.8	34.2	34.2	15.5	2.8	10.8	0.0	39.7
	2-methyl-1-butene	30.3	9.1	1.0	1.0	50.9	0.0	78.5	0.0	34.5
	2-methyl-1-pentene	10.6	3.2	–	–	5.0	0.0	10.4	0.0	5.3
	2-methyl-2-butene	6.0	1.8	–	–	9.3	0.0	21.2	0.0	31.2
	2-methyl-2-pentene	2.1	0.6	0.6	0.6	–	–	–	–	–
	2-methylheptane	7.1	2.1	–	–	8.6	0.0	5.4	0.0	11.2
	2-methylhexane	6.7	2.0	–	–	29.3	0.0	8.3	0.0	26.1
	2-methylpentane	50.2	15.1	1.0	1.0	–	2.1	11.1	0.0	22.0
	2,2-dimethylbutane	1.5	0.5	–	–	62.7	0.0	19.3	0.0	0.0
	2,3-dimethyl-2-pentene	7.5	2.3	1.0	1.0	14.3	0.0	5.1	0.0	18.7
	2,3-dimethylbutane	2.8	0.8	2.0	2.0	52.4	4.4	15.8	0.0	76.4
	2,3,4-trimethylpentane	5.3	1.6	–	–	8.2	0.0	27.2	0.0	30.8
	2,4-dimethylpentane	–	–	–	–	2.5	0.0	18.8	0.0	24.5
	3-ethyltoluene	15.8	4.7	–	–	8.8	0.5	33.8	0.0	24.5
	3-methyl-1-butene	29.5	8.9	–	–	–	–	–	–	–
	3-methylheptane	5.7	1.7	2.9	2.9	–	0.8	5.8	0.0	5.6
	3-methylhexane	24.5	7.4	–	–	2.5	0.8	9.3	0.0	20.3
	3-methylpentane	12.5	3.8	–	–	4.5	0.0	7.2	0.0	30.7
	4-ethyltoluene	7.7	2.3	3.1	3.1	26.3	0.0	64.4	0.0	85.4
	4-methyl-1-pentene	27.2	8.2	0.7	0.7	–	–	–	–	–
	4-methylheptane	5.6	1.7	1.8	1.8	–	0.0	9.1	0.0	8.9
	a-pinene	6.2	1.9	–	–	16.9	0.8	85.7	0.0	78.6
	acetylene	2858.9	857.7	9.2	9.2	834.9	36.3	839.3	10.9	1080.9
	benzene	232.0	69.6	72.4	72.4	273.2	4.7	123.2	0.7	282.2
	butane	24.8	7.4	29.2	29.2	38.9	0.0	252.3	1.4	366.0
	butylbenzene	8.5	2.6	–	–	5.0	0.5	108.5	0.0	16.9
	c-1,3-dimethylcyclopentane	–	–	–	–	0.7	0.0	11.8	0.0	2.8
	c-2-butene	11.7	3.5	0.9	0.9	14.7	0.5	85.5	1.0	78.9
	c-2-hexene	6.1	1.8	14.4	14.4	17.8	0.0	16.9	0.0	36.7
	c-2-pentene	8.4	2.5	–	–	59.6	0.0	66.9	0.0	45.3
	c-3-hexene	7.2	2.2	–	–	–	–	–	–	–
	cyclohexane	51.9	15.6	–	–	1.5	0.0	57.2	0.0	4.7
	cyclohexene	14.5	4.4	3.7	3.7	4.4	0.0	4.3	0.0	18.2

ACPD
12, 9945–9983, 2012

Table 2. Continued.

	Species	CFM56-JP8				T63-JP8		T63-FT		T63-Blend
		Idle	Taxi	Landing	Takeoff	Idle	Cruise	Idle	Cruise	Idle
VOC	cyclopentane	12.6	3.8	1.8	1.8	26.5	0.0	34.1	0.0	18.9
	cyclopentene	95.5	28.7	–	–	1.9	0.0	23.6	0.0	16.0
	cyclopropane	2.9	0.9	–	–	–	–	–	–	–
	decane	2.5	0.8	33.4	33.4	5.3	9.1	173.1	0.0	231.4
	dodecane	108.3	32.5	16.1	16.1	–	–	–	–	–
	ethane	115.5	34.7	83.3	83.3	149.6	26.6	143.7	0.0	158.6
	ethene	77.3	23.2	28.1	28.1	2865.5	49.6	1379.7	8.8	2984.4
	ethylbenzene	3.9	1.2	1.0	1.0	24.1	0.0	59.2	0.0	75.3
	heptane	5.9	1.8	–	–	132.8	0.0	16.3	0.0	114.0
	hexane	15.4	4.6	2.4	2.4	231.9	66.9	26.9	0.0	149.9
	hexylbenzene	16.6	5.0	–	–	–	–	–	–	–
	i-butane	42.7	12.8	42.2	42.2	4.9	0.4	89.5	0.0	0.0
	i-butene	71.7	21.5	5.5	5.5	119.8	0.0	512.3	0.0	425.4
	i-pentane	34.0	10.2	29.9	29.9	0.0	0.0	0.0	0.0	270.7
	isoprene	56.0	16.8	–	–	82.3	0.0	38.6	0.0	5.0
	i-propylbenzene	4.8	1.4	0.8	0.8	8.3	0.0	102.6	0.0	90.5
	limonene/indan	7.9	2.4	–	–	0.0	0.0	0.0	0.0	0.0
	m-xylene	26.4	7.9	1.1	1.1	37.6	0.0	55.5	0.0	7.3
	methylcyclohexane	14.4	4.3	–	–	5.1	0.0	5.8	0.0	15.9
	methylcyclopentane	11.2	3.4	–	–	2.6	0.0	11.8	0.0	14.2
	naphthalene	45.9	13.8	1.6	1.6	–	–	–	–	–
	nonane	36.1	10.8	–	–	112.5	0.0	3.4	0.0	121.3
	o-xylene	5.2	1.6	–	–	24.1	0.0	66.4	0.0	80.9
	octane	7.5	2.3	0.9	0.9	14.9	0.0	3.4	0.0	21.7
	p-xylene	4.8	1.4	3.8	3.8	19.6	1.0	44.4	0.0	95.8
	pentane	12.0	3.6	15.6	15.6	12.3	0.0	60.9	0.0	4.6
	propane	37.4	11.2	32.6	32.6	30.3	0.0	15.5	0.0	13.9
	propene	696.2	208.9	6.3	6.3	1087.8	5.3	1120.6	13.0	1545.6
	propylbenzene	16.6	5.0	1.4	1.4	14.6	0.0	35.3	0.0	38.4
	propyne	72.3	21.7	–	–	84.0	0.7	97.6	0.1	123.3
	sec-butylbenzene	39.4	11.8	1.6	1.6	–	–	–	–	–
	styrene	8.2	2.5	–	–	12.4	0.0	7.5	0.0	24.2
	tetradecane	4.9	1.5	0.9	0.9	–	–	–	–	–
	toluene	84.7	25.4	3.0	3.0	108.5	1.5	34.0	0.3	98.6
	1,3-hexadiene (trans)	6.3	1.9	–	–	7.6	0.0	29.7	0.0	9.1
	t-2-butene	61.0	18.3	4.3	4.3	53.0	1.1	116.8	0.4	108.2
	t-2-hexene	9.5	2.9	–	–	9.9	0.0	13.0	0.0	13.4
	t-2-pentene	15.7	4.7	–	–	102.1	0.0	28.2	0.0	138.4
	tridecane	47.4	14.2	1.9	1.9	–	–	–	–	–
	undecane	93.7	28.1	15.8	15.8	2.2	2.5	45.4	0.0	99.1
POC	$C^* = 10^{-2}\,\mu g\,m^{-3}$	4.8	1.7	3.2	2.1	31.0	0.3	21.8	3.8	17.6
	$C^* = 10^{-1}\,\mu g\,m^{-3}$	4.8	2.8	4.4	3.1	48.6	0.5	38.1	6.1	27.6
	$C^* = 10^{0}\,\mu g\,m^{-3}$	6.4	3.4	4.7	3.8	24.7	0.2	28.7	7.7	18.7
	$C^* = 10^{1}\,\mu g\,m^{-3}$	4.8	10.6	7.0	4.5	61.8	0.6	76.6	14.0	56.4
	$C^* = 10^{2}\,\mu g\,m^{-3}$	4.8	23.5	7.0	4.9	85.5	0.8	118.8	3.1	73.6
	$C^* = 10^{3}\,\mu g\,m^{-3}$	11.2	158.8	16.4	13.4	15.0	0.1	1.8	0.0	8.0
	$C^* = 10^{4}\,\mu g\,m^{-3}$	25.6	285.1	10.4	8.4	56.2	0.5	9.7	0.0	26.6
	$C^* = 10^{5}\,\mu g\,m^{-3}$	80.0	34.1	4.0	5.9	984.0	9.4	196.3	12.6	493.3
	$C^* = 10^{6}\,\mu g\,m^{-3}$	1459.4	39.1	20.0	11.3	4901.3	46.6	3613.6	12.4	3814.1
	$C^* = 10^{7}\,\mu g\,m^{-3}$	1459.4	39.1	20.0	11.3	4901.3	46.6	3613.6	12.4	3814.1

ACPD
12, 9945–9983, 2012

Table 3. VBS yields for POCs for non-idle and idle emissions.

POC C^*	Non-idle yields				Idle yields			
	$C^* = 10^0$ $\mu g m^{-3}$ (a_1)	$C^* = 10^1$ $\mu g m^{-3}$ (b_1)	$C^* = 10^2$ $\mu g m^{-3}$ (c_1)	$C^* = 10^3$ $\mu g m^{-3}$ (d_1)	$C^* = 10^0$ $\mu g m^{-3}$ (a_1)	$C^* = 10^1$ $\mu g m^{-3}$ (b_1)	$C^* = 10^2$ $\mu g m^{-3}$ (c_1)	$C^* = 10^3$ $\mu g m^{-3}$ (d_1)
$10^3\,\mu g m^{-3}$	0.000	0.310	1.000	0.000	0.195	0.000	0.863	0.000
$10^4\,\mu g m^{-3}$	0.000	0.089	1.000	0.000	0.085	0.000	0.994	0.000
$10^5\,\mu g m^{-3}$	0.000	0.000	0.302	0.000	0.000	0.000	0.938	0.000
$10^6\,\mu g m^{-3}$	0.000	0.000	0.034	0.000	0.000	0.000	0.601	0.000
$10^7\,\mu g m^{-3}$	0.000	0.000	0.001	0.000	0.000	0.000	0.370	0.000

ACPD
12, 9945–9983, 2012

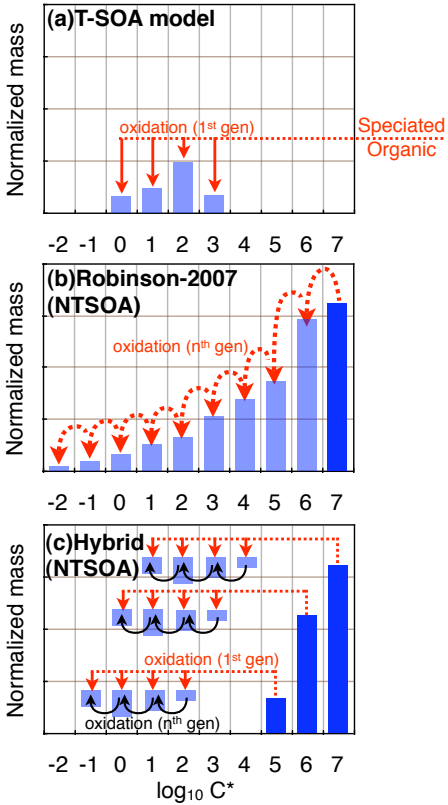

Fig. 1. Schematics that demonstrate the SOA mechanism for the T-SOA model, Robinson-2007 method and Hybrid method.

ACPD
12, 9945–9983, 2012

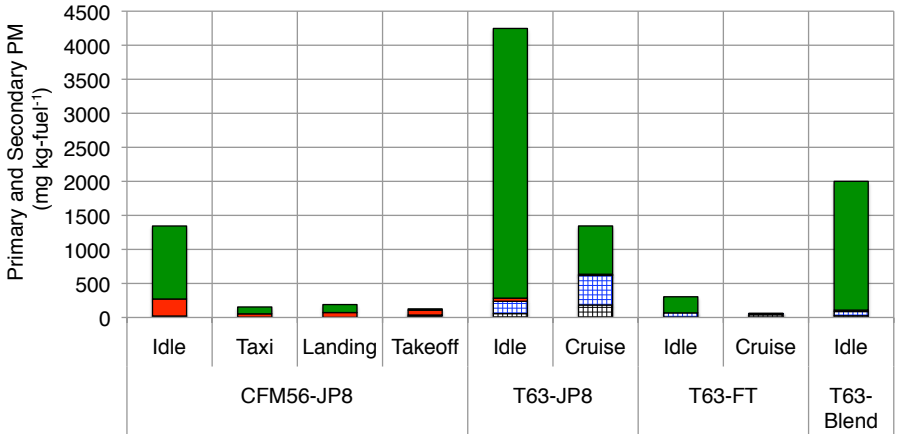

Fig. 2. Average black carbon, POA, sulfate and SOA from aircraft exhaust across the two field campaigns. CFM56 and T63 are gas turbine engines. JP8 is a petroleum-based aviation fuel, FT is a Fischer-Tropsch fuel derived from coal and Blend is a 50:50 JP8:FT mixture.The results for CFM56-JP8-Idle are the average of three independent experiments and the results for T63-JP8-Idle are the average of two independent experiments. We did not perform a cruise experiment for T63-Blend.

ACPD
12, 9945–9983, 2012

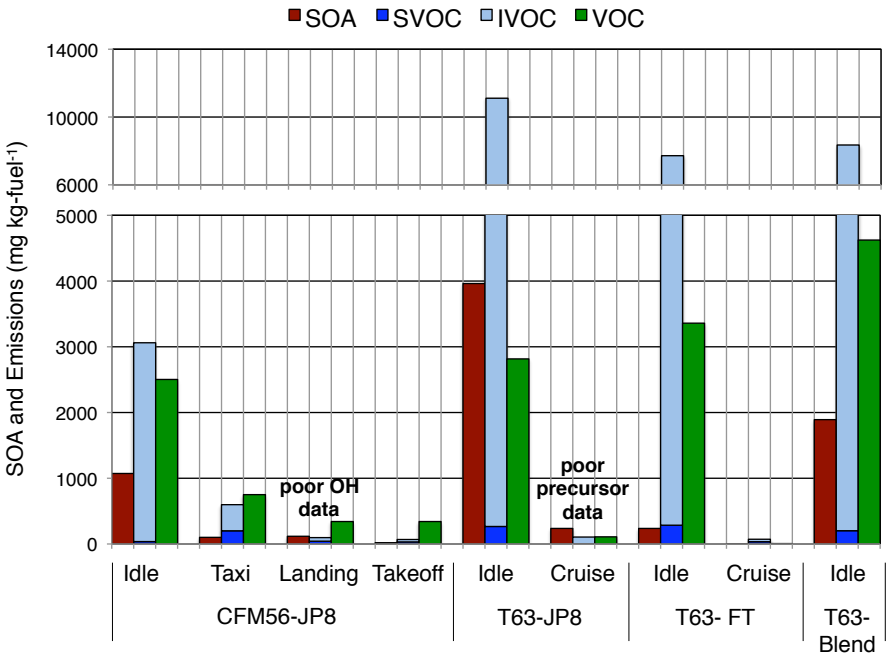

Fig. 3. Average emission factors for SOA, POC (SVOC and IVOC) and VOC (SOA precursors) across the two field campaigns. The results for T63-JP8-Idle are the average of two independent experiments. We did not perform a cruise experiment for T63-Blend.

ACPD
12, 9945–9983, 2012

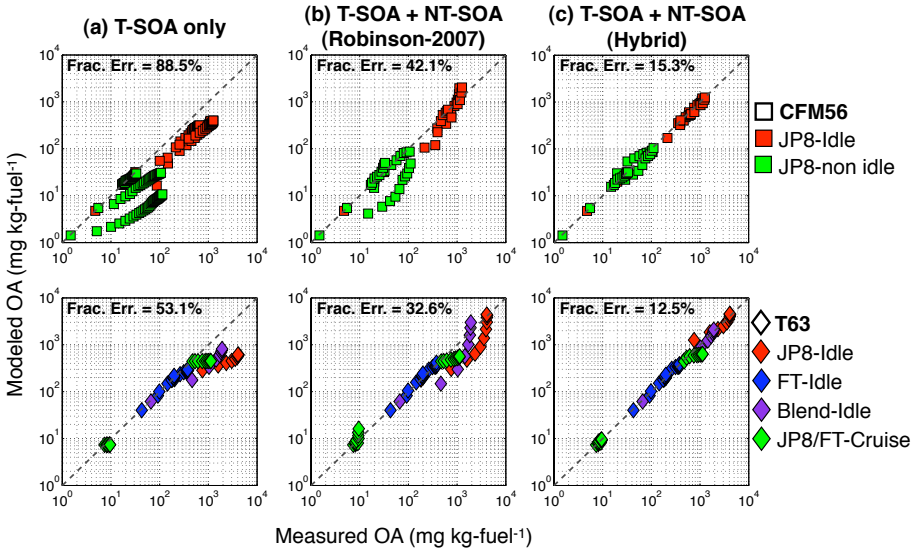

Fig. 4. Modeled vs measured OA mass for the T-SOA model and two versions of the NT-SOA model (Robinson-2007 and Hybrid). The top row shows experiments done on the CFM56 engine and the bottom row shows experiments done on the T63 engine.

ACPD
12, 9945–9983, 2012

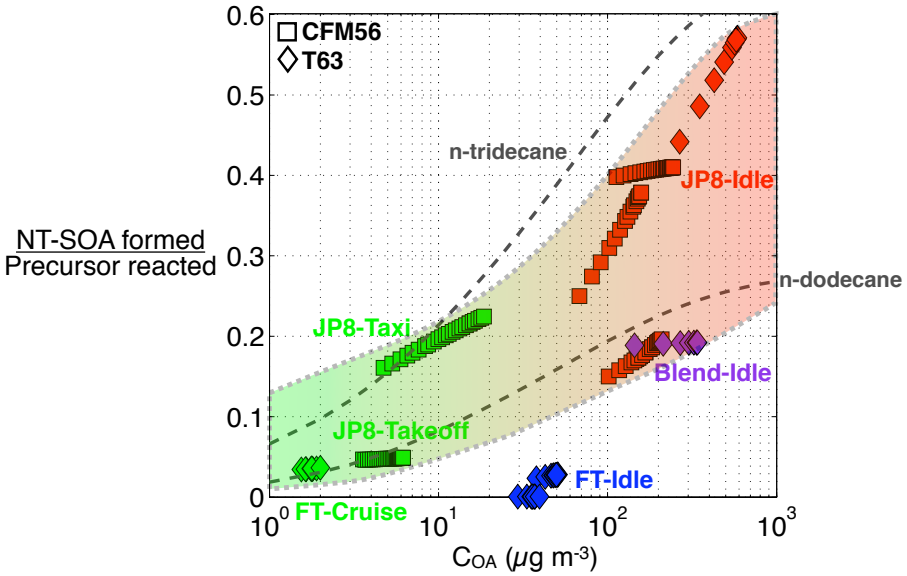

Fig. 5. NT-SOA yield plotted as a function of C_{OA}. For reference, we also include SOA yields for *n*-dodecane and *n*-tridecane (dotted grey lines).

ACPD
12, 9945–9983, 2012

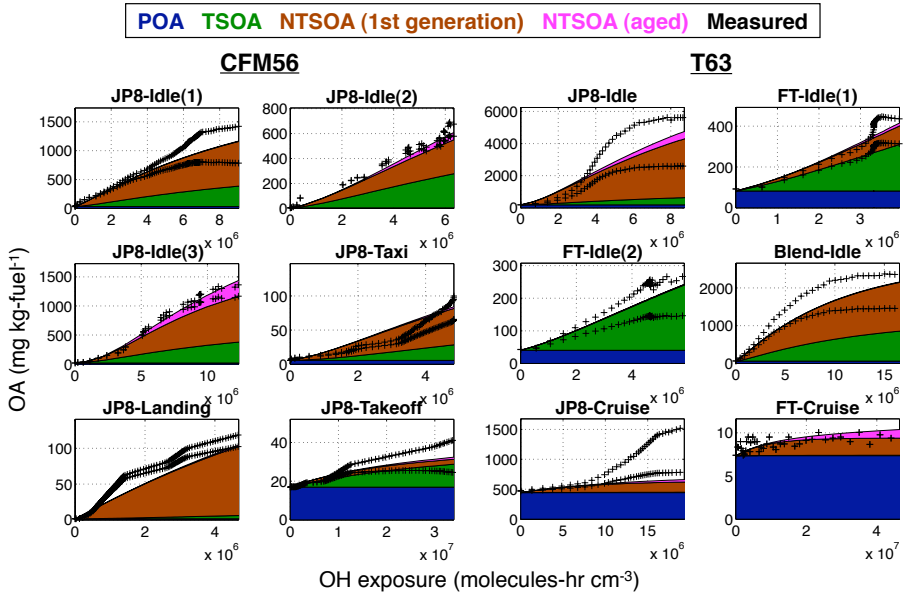

Fig. 6. Model predictions of OA compared to those measured during the experiment. NT-SOA is predicted using the Hybrid method using best fits for each experiment.

ACPD
12, 9945–9983, 2012

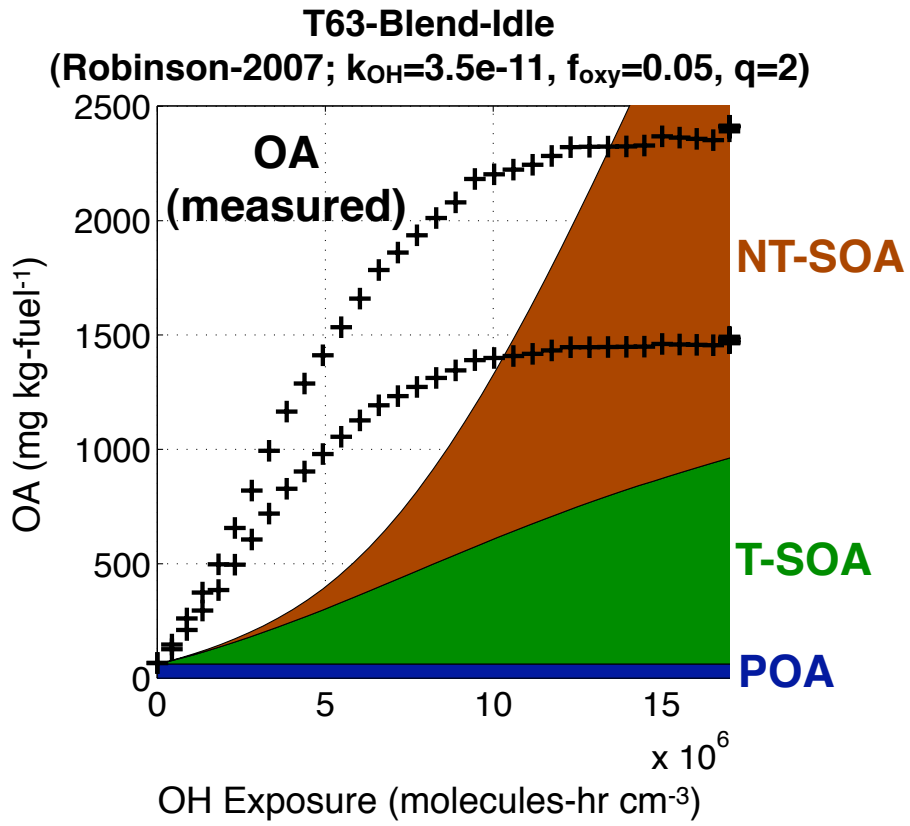

Fig. 7. Measured OA compared to model predictions using best-fits of the Robinson-2007 method for the T63-Blend-Idle experiment.

ACPD
12, 9945–9983, 2012

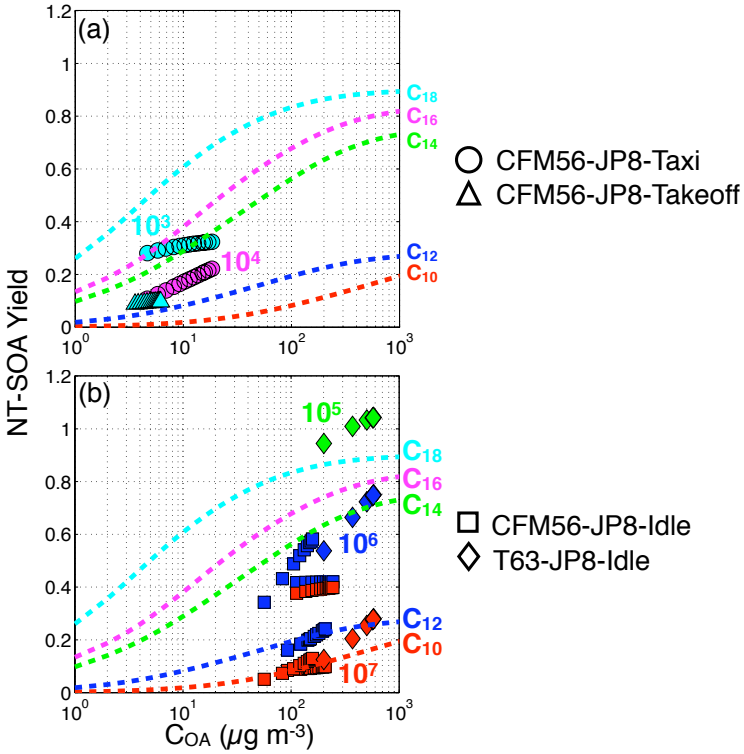

Fig. 8. SOA yield plotted for POC precursors that contribute more than 15 % of NT-SOA mass as a function of C_{OA} (symbols). For reference, we also plot SOA yields for *n*-decane (estimated), *n*-dodecane, *n*-tetradecane, *n*-hexadecane and *n*-octadecane (estimated) (dotted lines). The different colors connect the symbols to the dotted lines. For example, the SOA yields for the $C^* = 10^6\,\mu g\,m^{-3}$ bin for all the experiments are plotted with blue squares and the SOA yield for C^* equivalent *n*-dodecane (C_{12}) is plotted with a blue dotted line.

ACPD
12, 9945–9983, 2012